Acta Astronautica 223 (2024) 1–14

Contents lists available at ScienceDirect

Acta Astronautica

journal homepage: www.elsevier.com/locate/actaastro

Research paper

Combustion behavior of NMP-001, a nitromethane-based green rocket propellant

Maxim Kurilov *, Lukas Werling, Christoph Kirchberger, Helmut Ciezki, Stefan Schlechtriem

DLR Institute of Space Propulsion, Im Langen Grund, Hardthausen a. K., 74239, Germany

ARTICLE INFO

Keywords:
Nitromethane
Green propulsion
Spacecraft
Satellite
New space
RCS
DACS
Hydrazine replacement
Monopropellant
Characteristic length
Combustion efficiency

ABSTRACT

Hydrazine's carcinogenic and toxic nature makes its use in space propulsion expensive and necessitates careful launch campaign planning, which may cause delays. One already established alternative is to use energetic salt-based ionic solution propellants. However, the costs remain high because these salts are costly and highly regulated energetic materials. Additionally, propellants based on these energetic salts produce much higher temperatures during decomposition and combustion, as is the case for hydrazine. Consequently, expensive refractory metal-based alloys and high-temperature oxidation-resistant catalytic reactors must be used, which further drives up the costs. Alternatively, hydrogen peroxide may be used, though only in applications with a low specific impulse requirement. This study explores an alternative approach: using nitromethane, a commonly available laboratory solvent. NMP-001 is a nitromethane-based monopropellant that contains additives that allow for low-pressure combustion and reduce sensitivity to mechanical stimuli. Multiple combustion chamber configurations with varying characteristic lengths were tested in rocket combustion experiments. With the 11.5 m L^*-configuration, a 15.1 bar low-pressure limit could be determined. The 7.3 and 5.0 m L^*-configurations yielded a 16.2 and 28.3 bar low-pressure combustion limits, respectively. These outcomes are significantly below the 30 bar limit reported in the literature. Despite using only a simple heat-sink combustion chamber with a non-sophisticated injector element and a non-optimized propellant formulation, combustion was 83 to 95 % efficient with a C* ranged between 1133 to 1302 m/s. These figures are higher than for hydrogen peroxide and are comparable to the theoretical performance of state-of-the-art green liquid monopropellants.

1. Introduction

1.1. Green propulsion

The satellite, spacecraft, and defense industries have seen a significant rise in propulsion technologies aimed at replacing hydrazine as the dominant monopropellant for station-keeping, RCS (reaction control system[1]), DACS (divert and attitude control system) and other orbital control and propulsion applications. The main reason is hydrazine's toxicity and ability to cause cancer [1]. These properties require extensive safety measures while handling this substance. Such measures, for example, involve the use of space-suit-like SCAPE-suits that feature external breathing-air support. Equipment like this and the training associated with using these items require high capital investment and careful mission planning to avoid delays during launch preparation of space missions. Especially in the current era of "New Space", where many private actors participate in the development, production, launch, and operation of satellites and spacecraft, more cost-efficient alternatives for hydrazine seem to be quite beneficial and thus desirable. Potential overall system cost savings of up to 66% are attributed by Marshall and Deans [2] if an alternative monopropellant is used instead of hydrazine. Bombelli et al. [3] argue that cost savings may be exceptionally high in satellite constellations. At least three research streams are being pursued within the space propulsion community to create alternative liquid monopropellants to compete with hydrazine. In two cases a solid oxidizer salt is combined with water as a solvent and phlegmatizer and in the last case highly concentrated hydrogen peroxide is used.

One approach, which uses a solid oxidizer salt, is rooted in Europe. It involves using ammonium dinitramide (ADN) as the energetic oxidizer salt. This component is first dissolved in water, then stabilizers

* Corresponding author.
E-mail addresses: maxim.kurilov@dlr.de (M. Kurilov), lukas.werling@dlr.de (L. Werling), christoph.kirchberger@dlr.de (C. Kirchberger), helmut.ciezki@dlr.de (H. Ciezki), stefan.schlechtriem@dlr.de (S. Schlechtriem).

[1] See Nomenclature.

https://doi.org/10.1016/j.actaastro.2024.06.046
Received 27 March 2024; Received in revised form 19 June 2024; Accepted 23 June 2024
Available online 1 July 2024
0094-5765/© 2024 DLR - Deutsches Zentrum für Luft- und Raumfahrt e.V. - German Aerospace Center. Published by Elsevier Ltd on behalf of IAA. This is an open access article under the CC BY-NC-ND license (http://creativecommons.org/licenses/by-nc-nd/4.0/).

Nomenclature

ADN	Ammonium dinitramide
DACS	Divert and attitude control system
DSC	Differential scanning calorimetry
FS	Full scale
HAN	Hydroxylammonium nitrate
HR	Heating rate, [K/ms]
NM	Nitromethane
OI	Oscillation intensity, [%]
PLC	Programmable Logic Controller
PR	Pressure rate, [%]
SMD_{est}	Estimated Sauter-Mean-Diameter, [μm]
A_t	Nozzle throat area, [m^2]
A_{cc}	Combustion chamber cross-section area, [m^2]
C^*	Characteristic velocity, [m/s]
C^*_{CEA}	Calculated theoretical characteristic velocity, [m/s]
d_t	Nozzle throat diameter, [m]
d_{inj}	Injector orifice diameter, [m]
L^*	Characteristic chamber length, [m]
Ma	Mach number
Oh	Ohnesorge number
P_{tank}	Propellant tank pressure, [bar]
Q	Arbitrary data array
Re	Reynolds number
u	Injector jet exit velocity, [m/s]
V_c	Volume of the combustion chamber, [m^3]
We	Weber number
η_{C^*}	Combustion efficiency, [%]
μ	Dynamic viscosity, [Pa s]
σ	Surface tension, [N/m]

and fuel-like components such as ammonia, methanol, and monomethyl formamide are added. Negri et al. [4] and Wingborg et al. [5] thoroughly analyzed the LMP-103S and FLP-106 propellants. Additionally, LMP-103S was tested in orbit on the PRISMA satellite [6] and is now used as an orbital propellant [7].

In another approach mainly focused on in Japan and the USA, hydroxyl ammonium nitrate (HAN) is the oxidizer component. First, this energetic compound is dissolved in water, and then fuel components are added. The Japanese SHP-163 propellant was first demonstrated on a high-altitude-dropped plane-like vehicle [8] and then in orbit on board the RAPIS spacecraft [9]. AF-M315, now called ASCENT, was developed by the U.S. Air Force [10,11]. This propellant was also demonstrated in orbit as part of the GPIM mission, which featured a 1 N AF-M315 thruster system [10,12]. In HAN and ADN-based thrusters, heated solid catalyst beds are usually employed to trigger propellant decomposition and ignition.

Despite the progress, shortcomings persist in both approaches. Due to their high combustion temperature, both HAN- and ADN-based propellants necessitate materials capable of withstanding high temperatures for the combustion chamber, catalyst base material, and active phase, thereby increasing system costs. Furthermore, in both cases, catalysts require preheating to higher temperatures compared to hydrazine thrusters [4,10,13–16]. Coupled with the high cost of propellants,[2] these characteristics may explain the limited adoption of these propellants today [16,19].

A third approach is to use hydrogen peroxide in various concentrations. Although this substance was already used during the 1930s and 1940s as a rocket propellant in the Me-163 warplanes, the A4 ballistic missile, and other applications, it was sparsely used, in Western space programs between the Second World War and the 1990s. Ventura et al. [20] attribute this to the negative framing in the literature and anecdotal reports of accidents and incidents with hydrogen peroxide caused by its uncontrolled decomposition and detonation. An additional drawback commonly attributed to hydrogen peroxide is its insufficient storability due to the decay of concentration (hydrogen peroxide slowly decomposes into water and oxygen). In their article, the authors combat some of the long-standing prejudices concerning detonability and present evidence that demonstrates the stability of modern rocket-grade hydrogen peroxide to be sufficient for use in spacecraft and rockets. In the former Soviet Union, however, hydrogen peroxide was used not only with the Soyuz rocket power pack [21] but also on some versions of the Soyuz capsule [22,23]. Since the early 2000s, the pace of hydrogen peroxide propulsion research has increased significantly. Numerous academic and commercial research groups have published on the topic. One notable application is hydrogen peroxide thrusters for attitude control and propulsion in small satellites. Pasini et al. [24] present a 0.5 N propulsion system for a 3U CubeSat. Higher thrust systems are also being worked on [25]. In this article, Surmacz et al. also address another critical topic in this field: given the widespread availability of 98% hydrogen peroxide in recent years, there is a pressing need to develop novel heat-resistant catalytic materials to facilitate its decomposition, making additional research and development necessary. Due to their low melting point, traditional silver-based catalysts are limited to accommodating hydrogen peroxide concentrations ranging from 85% to 90% [25]. The storability of hydrogen peroxide is still of concern despite the progress made since the 1960s, which has significantly reduced its decomposition rate. The lifespan of propulsion systems utilizing hydrogen peroxide remains restricted, necessitating additional cooling measures to mitigate decomposition [26,27]. Even though hydrogen peroxide only offers a lower specific impulse performance than hydrazine (see Fig. 1), its high density (1430 kg/m^3) offers a benefit in volume-restricted systems. This makes hydrogen peroxide usable in specific niche applications such as CubeSats.

1.2. Research on nitromethane

Nitromethane has been considered a promising rocket propellant since the 1930s [28,29]. In the 1940s and 1950s, research programs carried out by the U.S. defense agencies aimed at developing nitromethane-powered rocket chambers and gas generators [29,30]. In the 1950s, further studies were published by Israeli researchers. Because of the relatively large characteristic length requirement[3] that was necessary to enable stable, self-sustaining combustion, only a limited propellant quantity is available per chamber unit area for cooling in a motor cooling jacket, which commonly led to explosions described as reported by [31,32]. The following Equation defines the characteristic length:

$$L^* = \frac{V_c}{A_t} \tag{1}$$

L^* : Characteristic chamber length, [m]

V_c : Volume of the combustion chamber, [m^3]

A_t : Nozzle throat area, [m^2]

During the 1960s to 2000s, nitromethane (NM) was neglected as a rocket propellant. However, in the 1980s, Benziger [33,34] recognized

[2] $>1000\frac{\$}{kg}$ for ADN-based [17], and $>700\frac{\$}{kg}$ for HAN-based propellants [18]

[3] 6 m for pure nitromethane, up to 25.8 m for propellant mixtures [31]

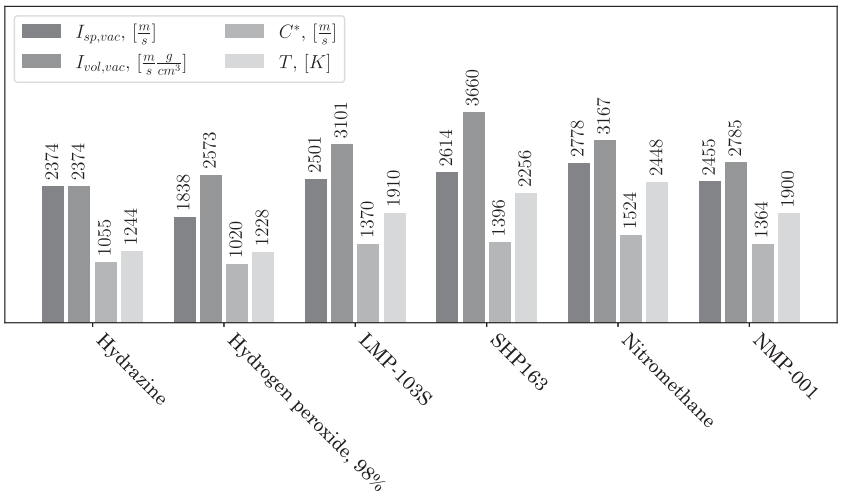

Fig. 1. Green propellant performance parameters, at 10 bar combustion pressure and a nozzle area ratio of 50:1. Figures for hydrazine derived from [38] assuming a 55% ammonia disassociation. The other figures were calculated with NASA CEA (see [39] for further details), assuming frozen flow.

its potential as a possible low-toxicity alternative to hydrazine, offering a higher performance. This research was focused on characterizing various transitional metal catalysts for nitromethane decomposition to enable similar decomposition and ignition as in hydrazine thrusters. Later, Kelzenberg et al. [35] and Boyer et al. [36] thoroughly evaluated nitromethane's combustion and decomposition behavior in strand burner experiments. In another publication Boyer et al. also analyzed and confirmed nitromethane's potential for use in propulsion systems [28]. Later, Yetter et al. [37] conducted combustion experiments utilizing pure nitromethane in a micro-scale combustion chamber with a diameter of 5 mm and a volume of 106 mm^3. The chamber was preheated using either a methane/air or a methane/oxygen flame for over a minute. Subsequently, nitromethane was introduced into the chamber alongside these gases. Stable operation was achieved at 24 bar after extinguishing the pilot flame.

Despite the challenges mentioned above, nitromethane exhibits excellent potential as an alternative to hydrazine due to its low toxicity, promising performance figures, and wide availability. Fig. 1 compares the adiabatic combustion temperature (T), the specific impulse ($I_{sp,vac}$), the volume-specific impulse ($I_{vol,vac}$), and the characteristic velocity (C^*) of hydrazine and common green propellants, nitromethane and NMP-001, a nitromethane-based green propellant presented in this paper. Nitromethane offers a similar specific impulse to HAN- and ADN-based formulations and is superior to hydrogen peroxide and hydrazine.

ADN and HAN are energetic, non-stable substances and require extensive care to avoid detonation or deflagration due to shock, friction, or electrostatic discharge during production and handling [40–42]. Even though nitromethane is also known to have energetic material-like properties [43], it is routinely handled in laboratories and industrial facilities [44]. It does not require special logistics and can be ordered online from standard chemical component distributors such as Sigma-Aldrich or Merck.

While substantial production upscaling may circumvent the high per-kg costs of ADN- and HAN-based propellants (see [17,18] for cost figures), such an enterprise requires substantial investments. Nitromethane's production is, however, already scaled up [44]. Moreover, this substance is a staple laboratory and industrial solvent, thus widely available in bulk quantities. Table 1 presents the most important physical properties of nitromethane. Special mention should be made of the low melting point, which eases thermal requirements on satellites and spacecraft and simplifies logistics.

In prior publications, researchers reported ignition and stable combustion challenges at pressures below 30 bar in case of a cold start or below 24 bar if the chamber is preheated [29,37,46,47]. These difficulties were primarily attributed to the decomposition mechanism of nitromethane. The CH_3-NO_2 bond's initial scission is one of the most important initial steps in nitromethane thermolysis. This reaction relies on intermolecular collisions. Therefore, higher pressure benefits nitromethane decomposition [35,37,48]. Kelzenberg et al. [35] and Boyer et al. [36] observed a disproportionate increase in burning rate with higher pressures, thus further cementing this hypothesis.

Table 1
Physical properties of nitromethane.
Source: Data from [45].

Formula	CH_3NO_2
Molar weight	61.041 g/mol
CAS RN	75-52-5
Melting point	−28.3 °C
Boiling point	101.2 °C
Density	1137 kg m^{-3}
Viscosity (25 °C)	0.63 mPa s
Enthalpy of formation	−112.6 kJ/kg
Vapor pressure (25 °C)	4.79 kPa

To enhance decomposition and thus help with the ignition and combustion of nitromethane, Bellinger et al. and Kindsvater et al. proposed to dissolve transition-metal salts and other catalysts in nitromethane [46,47]. As the source of ignition, Bellinger et al. [46] used a pyrotechnical "flamethrower-like" initiator, while Kindsvater et al. [47] reported on a pilot nitromethane-oxygen pilot-flame in a separate chamber utilized to initiate combustion in the main chamber. Subsequent laboratory investigations by Benziger [33,34] explored a catalytic approach to nitromethane exothermal decomposition. Although pure nitromethane could be successfully decomposed over Ni- and Cr-based materials, these catalysts were prone to deactivation due to carbon deposition. As a result, our research group opted to use a pilot flame for initiation and, similar to the sources mentioned above, incorporated a catalytic substance to facilitate nitromethane decomposition. The need for suitable catalysts led to a screening focused on finding and characterizing various candidate substances. The most significant findings of this study indicated that the addition of 2 wt% ferrocene, iron-(III)-acetylacetonate, or vanadyl-(III)-acetylacetonate caused the decomposition peak in closed-crucible differential scanning calorimetry (DSC) measurements to shift by 100, 65, and 61 °C, respectively, compared to pure nitromethane (384 °C) [49].

As mentioned, nitromethane is an energetic substance capable of deflagration and detonation, especially if confined or heated [46,50]. To alleviate this, inert substances – or phlegmatizing agents – can be

Table 2
Composition of NMP-001.

Nitromethane	Carl Roth, 98.5%	85 wt.%
Dimethyl sulfoxide	Carl Roth, 99.8%	13 wt.%
Ferrocene	Sigma-Aldrich, 98%	2 wt.%

added to nitromethane-based propellant mixtures [28,29,46]. In [43], a screening of such substances is presented, and their effect on the impact sensitiveness of nitromethane is characterized. The most important finding was that low wt.%-admixtures of n-butanol, and dimethyl sulfoxide can decrease BAM-Fallhammer impact sensitiveness from ⩽5J to >10 J. The additions, however, also caused a decrease in performance compared to pure nitromethane.

This paper presents a rocket combustion chamber study with the NMP-001 propellant. This formulation is considered "green" according to the definition provided in [51]: It does not contain substances that are harmful upon contact with the skin or any components that have been proven to cause cancer, genetic effects, or fertility damage. NMP-001 contains 85 wt% nitromethane, a small quantity of ferrocene that serves as an ignition catalyst, and dimethyl sulfoxide, which is included as a phlegmatizer to reduce the risk of unintended initiation in the propellant line or detonative combustion. The added amount of phlegmatizer was tailored to ensure an impact sensitivity above 10 J. This internal requirement is a prerequisite for safely handling large amounts of NMP-001 during test-bench operation. Both additives were characterized in our previous research [43,49]. Table 2 presents the quantities used and the suppliers from which the chemicals are procured.

As a prototype propellant, NMP-001 does not possess all the desirable characteristics necessary for a usable propellant. For instance, it exhibits a low-temperature limit only slightly above 10 °C. Below this temperature, precipitation of ferrocene from the solution occurs. Moreover, comprehensive safety evaluations such as Koenen and large-scale gap tests have not been conducted with this propellant thus far, aside from the BAM-Fallhammer impact sensitivity test. NMP-001 was solely developed to demonstrate the safe utilization of nitromethane as an alternative to hydrazine.

Additionally, its objective was to demonstrate combustion under pressures commonly encountered in pressure-fed propulsion systems used in satellites and spacecraft. In systems employing pressure-fed rocket motors, minimizing the combustion chamber pressure is advantageous to avoid the need for heavy, thick-walled propellant tanks required to maintain the additional pressure head. Consequently, to avoid incurring a system mass penalty due to excessively heavy tanks, thrusters utilized in pressure-fed satellite and spacecraft propulsion systems operate at low combustion chamber pressures, which can be as low as 3 bar [8].

Previous studies have indicated that the lowest feasible combustion chamber pressure for stable operation of a nitromethane-based propellant mixture is 30 bar in the case of a cold start [47] or 24 bar with preheating of the combustion chamber [37], which are higher than for hydrazine or its alternatives. This test campaign aims to assess if operation at lower pressures is possible with NMP-001. Additionally, the performance of this propellant was evaluated at different characteristic lengths L^*.

Due to the admixtures present, the performance of NMP-001 is inferior to that of pure nitromethane, with a theoretical specific impulse of 2841 m/s compared to 2584 m/s (see Fig. 1). Nonetheless, its performance remains comparable to that of LMP-103S, which yields a specific impulse of 2543 m/s.

2. Experimental setup

2.1. The M11.4 test bench

For the execution of the NMP-001 test campaign, the experimental setup depicted in Fig. 2 was integrated into the M11.4 test bench within the DLR M11 test complex located in Lampoldshausen, Germany. This test facility is equipped with a redundant Siemens PLC (Programmable Logic Controller) for control purposes. It includes high-pressure (up to 200 bar) H2, O2, N2, and air supply. Data acquisition is facilitated through a NI-PXI-based system capable of recording up to 160 sensor channels at a rate of up to 40 kHz. In the current configuration, up to 10 STS-TM pressure sensors with an accuracy of ⩽0.5% of the entire measurement range were utilized. Signals from these sensors are amplified using DEWETRON amplifiers before being processed by the data acquisition system.

For critical measurements such as the combustion chamber pressure (P_{cc}) and the ignitor pilot chamber pressure (P_{ign}), 100 bar full-scale (FS) sensors were employed, resulting in an uncertainty of ±0.5 bar for these readings. 200 bar FS sensors were used for all other measurements, introducing an uncertainty of ±1 bar for the respective quantities. The combustion chamber wall temperature was monitored using eleven 0.5 mm type K thermocouples with an accuracy of ±2.5 K. These thermocouples were strategically positioned along the combustion chamber axis as illustrated in Fig. 3, inserted into bores within the chamber wall, stopping 1.0 ± 0.05 mm before reaching the inner surface. To ensure consistent contact with the wall material, the thermocouples were loaded with a force of 2 N using springs (see Fig. 3), employing a methodology similar to that described in [52].

The propellant mass flow exiting the nitrogen-pressurized NMP-001 tank was measured using a RHEONIK RHM03L Coriolis flowmeter. This flowmeter ensures an accuracy of at least 0.5% of the measured value. The Siemens PLC regulates the pressure within the N_2, H_2, and O_2 reservoirs through controllable dome pressure reducers. Interchangeable orifice plates control the mass flow of oxygen and hydrogen gases.

A two-stage H_2/O_2 gas torch igniter was utilized to initiate combustion. This ignition method bears similarities to the one elucidated in [47], albeit with hydrogen replacing nitromethane to generate a pilot flame in the igniter pilot chamber. The pilot chamber operates in a hydrogen-rich environment (oxygen to hydrogen mass ratio ≈1). The mixture is ignited with the assistance of a spark plug and directed through a metal tube into the main combustion chamber (see Fig. 3). Upon entry into the main chamber, this hot mixture combines with additional oxygen from a separate pressure source, injected near the injector surface to enhance ignition. This injection of additional oxygen is referred to as boost oxygen.

2.2. Combustion chamber test setup

The combustion chamber (Fig. 2) is constructed from 1.4841 heat-resistant stainless steel, measuring 150 mm in length with an inner diameter of 22 mm. These dimensions are considered to have a length uncertainty of ±0.2 mm, accounting for manufacturing tolerances and potential elastic deformation and creep during the test campaign. Tests were conducted with the chamber positioned vertically to prevent propellant accumulations (see Fig. 2 on the left).

Several nozzles made from the CuCr1Zr high-temperature copper alloy were utilized during the test campaign. The inner diameters of these nozzles were selected to characterize performance at three distinct L^*-values: 11.7 m, 8.3 m, and 5.4 m (see Table 4). As will be discussed later, the nozzle throat area changed slightly in between the tests due to creep, deformation, and erosion. Therefore, in order to achieve high-quality results, the nozzle throat diameter was measured after cooling down the nozzle after each test. These measurements were carried out with precision gauges. Overall, the uncertainty of the nozzle throat cross section diameter is expected to be within ±0.04 mm.

It is noteworthy that this method of altering L^* is unconventional. Typically, to maintain flow conditions within the combustion chamber, L^* is adjusted by varying the length of the straight portion of the combustion chamber, as for example demonstrated by Werling and Hörger [53] or Khan and Qamar [54]. However, because it was

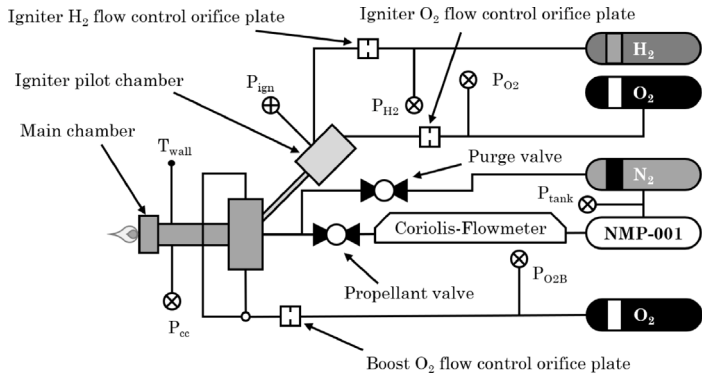

Fig. 2. NMP-001 test setup overview.

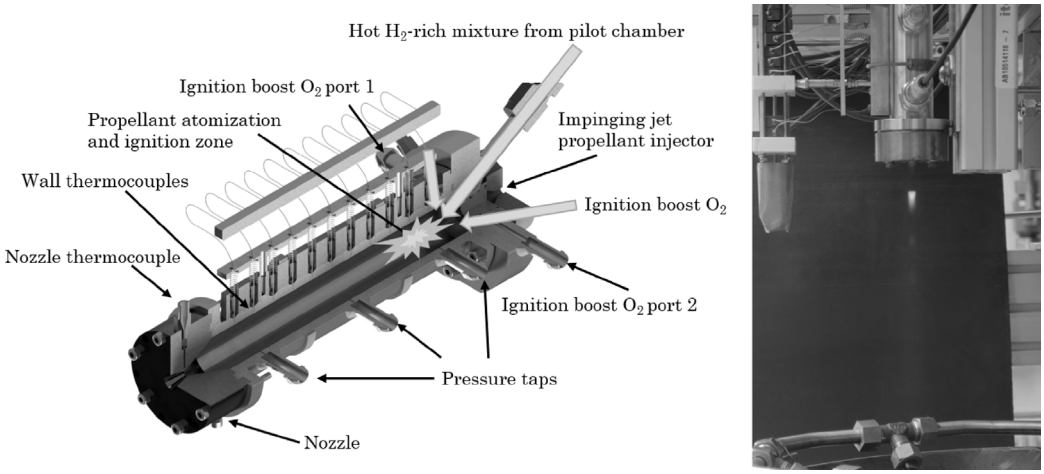

Fig. 3. Detail view of the combustion chamber test setup.

expected to significantly vary L^* in order to achieve stable combustion (L^* = 6 to 25.8 m as reported in [31,32,47]), it was deemed more pragmatic in the initial stages to modify L^* using multiple nozzles with differing throat diameters, rather than employing multiple large and lengthy combustion chambers with full instrumentation, which was considered prohibitively expensive and risky at this early developmental phase.

Despite the alteration of the flow field within the combustor by varying the critical nozzle cross-section area, the results are deemed comparable. This is primarily because the flow velocity in the straight portion of the chamber never reaches a significant fraction of the sonic velocity (see Table 4). Additionally, as outlined by Sutton and Biblarz [55] and by Gordon and McBride [56], the chamber-to-nozzle area ratio is sufficiently high for all test configurations to be considered infinite area combustors. Both references indicate that meaningful performance losses due to flow phenomena become relevant only if this area ratio falls below 3, a condition not found in the current study, as indicated in Table 4.

2.3. Propellant injection and atomization

For the injection and atomization of NMP-001, two geometrically similar 3D-triplet impinging jet injectors were employed. Both injectors were designed to generate a symmetrical flow field. Injector A, with an injector orifice diameter of 0.42 mm, was intended for lower mass flows. In contrast, injector B, with an orifice diameter of 0.58 mm, was designated for higher mass flow rates. Both injectors had an impingement half angle of 30°. The allocation of injectors to the combustor configurations is outlined in Table 4.

As part of the preparation for the combustion chamber test campaign, the injectors underwent cold-flow testing with water at ambient pressure and temperature conditions. A Malvern Spraytec device was utilized to measure the Sauter-Mean-Diameter (SMD) of the spray core. Measurements were taken 2 cm below the injector face. The results are illustrated in Fig. 4. In both injectors, the droplet size decreased as expected with increasing injector pressure drop, resulting in higher injection velocities. Power law relations describing the relationship between SMD and pressure drop were derived from these measurements and subsequently utilized for SMD estimation during test analysis.

As the combustor experiments conducted for this publication and presented in the subsequent sections were performed at combustion chamber pressures not exceeding the critical pressure of nitromethane (58.7 bar [45]), atomization plays an essential role in the combustion of the propellant spray [57]. The derived power law relations were employed to estimate the Sauter Mean Diameter (SMD) and assess the atomization degree's influence on the combustion test outcomes. However, it is crucial to note that the resulting SMD is only a rough approximation of the actual SMD prevalent during the combustion experiments. Therefore, the SMD will be referred to as SMD_{est} throughout the analysis.

The accuracy of this estimation is primarily constrained by the conditions under which the spray tests were conducted, i.e. a non-pressurized, non-reacting environment without heat transfer and vaporization effects. For instance, Hiroyasu and Arai [58] present measurements indicating that the droplet size produced by an air–diesel injector decreases below an effective injection pressure of 5 MPa with increasing ambient pressure. This injection condition was also the case in the presented test campaign. Although impinging jet injectors did not yield these specific measurements, it may be inferred that

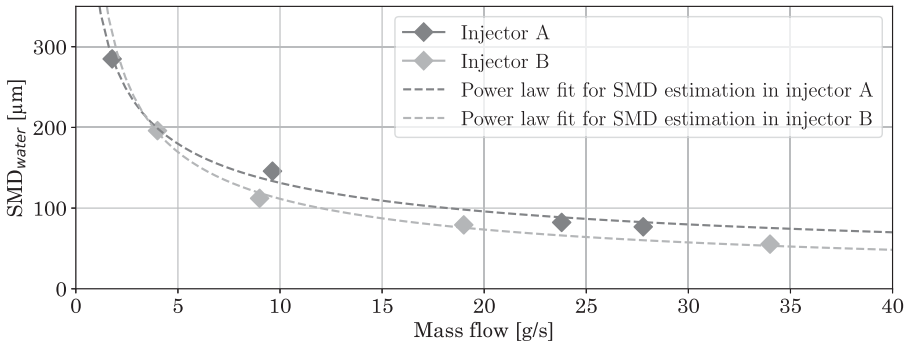

Fig. 4. Measured SMD values for injectors A and B and power law fits for SMD estimation.

the droplet formation process has similarities in its origins, as it is governed by the interaction between liquid structure and aerodynamic and viscous forces, which also influence spray formation in impinging jet injectors, see, e.g., [59]. Thus, it is evident that a general trend exists where a higher ambient pressure drop results in improved atomization, consequently leading to a smaller SMD.

Despite having slightly different flow properties, using water as a simulant liquid instead of NMP-001 is a valuable approach to grasping the injection and atomization behavior in the combustion chamber experiments. The following description shows comparable information about the expected spray behavior can be obtained. The atomization process in impinging jet injectors is governed by the dimensionless numbers Reynolds (Re), Weber (We), and Ohnesorg (Oh) [60–62]. These numbers are defined by the following Equations:

$$Re = \rho \frac{u d_{inj}}{\mu} \tag{2}$$

$$We = \rho \frac{u^2 d_{inj}}{\sigma} \tag{3}$$

$$Oh = \frac{\mu}{\sqrt{\rho \sigma d_{inj}}} \tag{4}$$

Re : Reynolds number
We : Weber number
Oh : Ohnesorge number
u : Jet exit velocity, [m/s]
d_{inj} : Injector orifice diameter, [m]
μ : Dynamic viscosity, [Pa s]
σ : Surface tension, [N/m]

The density of NMP-001 was measured to be 1135 kg/m^3 at 25 °C, which does not substantially deviate from the value of pure nitromethane. However, the surface tension and viscosity values for NMP-001 have yet to be determined. Therefore, the values for pure nitromethane were used for calculating the dimensionless numbers as a first estimate.

The Oh-numbers for each spray configuration and the We and Re ranges obtained during the spray experiments are presented in Table 3. This table includes values achieved in the experiments with water and values for nitromethane that would have been produced if this substance had been sprayed with the same injector at the same mass flow rates. Data for water are from [45].

Ciezki et al. and later Bailardi et al. [61,62], conducted a doublet impinging jet spray campaign with a large number of different Newtonian liquids. All three dimensionless numbers are connected via Eq. (5).

$$We = Oh^2 Re^2 \tag{5}$$

Thus, the Ohnesorge number, which is constant for a liquid and the chosen injector diameter in an experimental campaign, defines where spray results with a distinct liquid are positioned in the regime diagram We vs. Re, which these authors presented in their publications [61,62]. Consequently, liquids with similar Oh numbers show similar spray behavior. This is the case for nitromethane and water because their Oh numbers are nearly identical, as presented in Table 3.

Table 3
Spray parameters.

	Water	Nitromethane
Jet exit velocity	26–110 m/s	23–97 m/s
Oh	0.0043 and 0.0051	0.0040 and 0.0047
Re	12×10^3–72×10^3	17×10^3–1000×10^3
We	4×10^3–98×10^3	7×10^3–170×10^3

For liquids with Oh below approximately 0.02, the vigorous ruffled sheet ligament atomization regime was observed for We > 2000, Re > 5000, or the even more vigorous fully developed atomization regime above We ≈ 10 000 and Re ≈ 5000. In terms of comparability between nitromethane and water, this indicates that both liquids would atomize within the same regimes, considering the values presented in Table 3. Thus, it can be assumed with sufficient accuracy that the obtained water results can be transferred to NMP-001, making use of the presented injector setup.

Moreover, Lai et al. [63] report that regardless of the viscosity or surface tension of the test fluid, an impinging jet injector produces droplets of similar sizes at jet velocities exceeding 30 m/s, which is the case for most tests presented here.

2.4. Campaign overview and testing strategy

A test series was conducted for each of the three distinct L^*-values. Tests began with test configuration C1, which featured a characteristic length of 11.7 m. This L^*-value was chosen to create data comparable to the one reported by Kindsvater et al. [47] (L^* = 12.7 m).

After completing test series C1, it became foreseeable that the characterized propellant could also allow for stable low-pressure combustion at lower L^*-values. Therefore, for the next test series, it was decided to roughly half the characteristic length to L^* = 5.4 m (configuration C2). After completing the C2 test series, another L^* value, approximately between the C1 and C2 values, was picked for the C3 tests. After finishing the C3 test series, it was decided to generate additional data for higher-pressure combustion at moderately high L^* values. For these tests, designated as configuration C4, a nozzle with an initial L^* = 9.2 m was selected. The initial and final nozzle throat and L^* -values, along with the resulting variations of the Mach number inside the combustor for all test configurations, are presented in Table 4.

The testing strategy aimed at finding the low-pressure combustion limit was to set a certain tank pressure, carry out one experiment, and then, depending on the outcome, adjust the pressure to produce

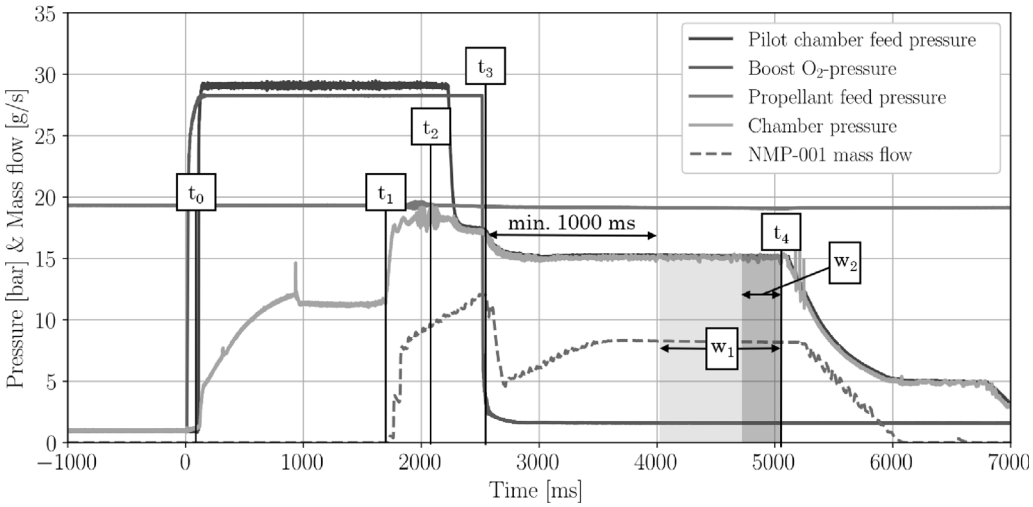

Fig. 5. Ignition and test sequence, and analysis logic (C1 test series test).

Table 4
Overview of test configurations, Mach number calculated with the finite area function combustion from [39].

	C1	C2	C3	C3
Injector	A	B	A	A
P_{tank} [bar]	17–44	60–90	25–90	70–90
L^* [m]	11.3–11.7	4.7–5.4	6.7–8.3	9.0–9.2
d_t [mm]	2.80–2.84	4.20–4.51	3.3–3.69	3.14–3.18
A_{cc}/A_t	60.0–61.7	23.8–27.4	35.6–44.4	47.8–49.1
Ma	0.007	0.023	0.015	0.008
Test runs	9	11	24	4

Table 5
Overview of test events.

Time	Event
−30 ms	Pilot chamber and boost oxygen valves actuated
0 ms	Pilot chamber hydrogen valve actuated, sparkplugs switched on
t_0	Torch full ignition: pressure rise onset in the chamber
t_1	NMP-001 injection: further pressure rise onset in the chamber
t_2	H_2 and O_2 valve closure: pilot chamber switched off
t_3	Boost O_2 valve closure: boost oxygen injection is switched off
t_4	NMP-001 valve switched off: flameout

a different propellant mass flow, producing a different chamber pressure. This procedure was carried out until the low-pressure limit in C1, C2, and C3 was found. Then, the experiments defining the low-pressure combustion limit were repeated twice to four times. If enough propellant from the used propellant batch was left, the other load points were also reproduced. This testing approach ensures that the low-pressure combustion limit is identified with high confidence and a wide range of combustion pressure load points is explored without introducing an additional possible source of variance using different propellant batches.

For the experiments that define the low-pressure combustion limits, at least two experiments were carried out with a high degree of repeatability (tank pressure deviation of ±1 bar, chamber pressure deviation <±10%). However, experiments could not always be repeated for some load points with a higher chamber pressure than the low-pressure combustion limit because the propellant ran out. In cases where only one hot-firing experiment was available per load point, the injector pressure drop to propellant mass-flow relation was used to verify consistency by comparing this value to data generated with water during the injector characterization cold-flow campaign.

2.5. Test sequence and analysis windows

Fig. 5 presents the key temperature and pressure data for a test with configuration C1 test at 19.1 bar tank pressure. This is a test in which the lowest possible chamber operation pressure was achieved in this campaign. The test data diagram for this test shall serve as an illustrative example to explain the test sequence used in the test campaign.

The test was initiated at t = 0 by activating the spark plug and thus initiating the pilot chamber. The pilot chamber oxygen valve and the ignitor boost oxygen valve, which controls the oxygen injection into the main combustion chamber, were operated with a slight oxygen lead to enable a smooth ignition. The hydrogen valve was also actuated at t = 0 ms. At t_0 (102 ms in this specific test), the pressure in the main chamber significantly increases due to the ignitor pilot chamber and ignitor boost oxygen operation, defining t_0 as the ignition point. The injection of NMP-001 followed at t_1. The interval between t_0 and t_1 was used to preheat the chamber to prevent hard starts. At t_2, the igniter pilot chamber was switched off, followed by the igniter boost stage at t_3 shortly after. In the case of this test, a stable monopropellant operation phase followed. After closing the main propellant valve at t_4, the combustion ceased. The experiment concluded with the injector and chamber being purged with nitrogen. Throughout all phases of the experiment, the combustion pressure was monitored by the control system. If an upper or lower pressure limit was reached, i.e., a redline was violated, the main valve was closed, the injector line was purged, and the propellant tank was depressurized. Table 5 presents an overview of the test events.

The ignition point t_1, the intervals between t_1, t_2, and t_3, the boost oxygen pressure, and the boost oxygen metering orifice were subject to changes in the test campaign to allow for a sure ignition at different chamber pressures. These variations influenced how much oxygen was injected into the combustor, resulting in changes in the total thermal energy applied to the chamber wall.

Consistent analysis windows were utilized to ensure a meaningful comparison between all experiments in all test configurations. The 1000 ms wide w_1-window was employed for calculating and evaluating the chamber wall heating and pressure change rates, because these quantities require a longer time to show sensible effects. In all tests, the window w_1 was positioned at least 1000 ms after the monopropellant operation initiation at t_3. This positioning was done to minimize the impact of the torch igniter on the combustion performance evaluation. A second window, which only features a 250 ms length, referred to as w_2, was placed in the last quarter of w_1. This window allowed for assessing dynamic effects caused by instabilities (i.e., the oscillation

Table 6
Stability rating criteria.

Criterion	Score change
Monopropellant combustion time <2000 ms	−2
Heating Rate (HR) <0, inside window w_1	−2
Oscillation intensity (OI) >5%, inside window w_2	−1
Combustion pressure change >5%, inside window w_1	−1
Outcome	**Test rating**
Stable combustion	3/3
Stable at least at pulse mode operation	2/3
Non-stable combustion	1/3

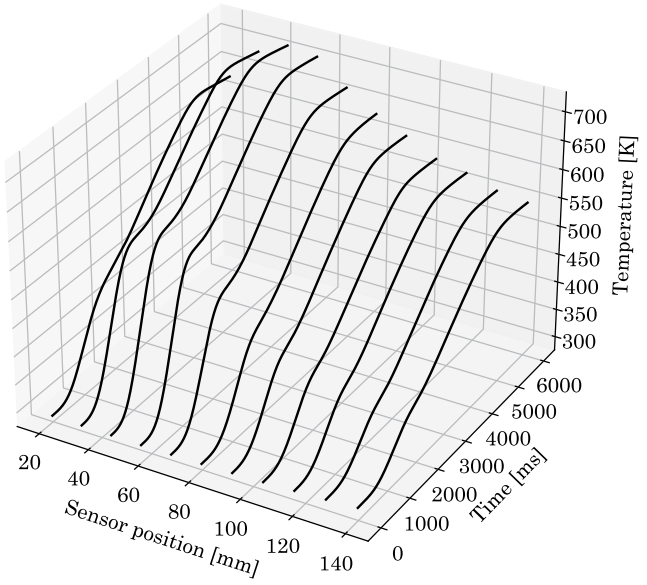

Fig. 6. Temperature data from a configuration C2 test.

intensity) and was also used for calculating the combustion efficiency. In some test runs with non-stable combustion, the interval between t_3 and t_4 was less than 2000 ms. In such cases, both windows were shortened to 250 ms and positioned right before the flameout at t_4.

2.6. Combustion behavior rating criteria

Assessing and rating the combustion stability is essential to determine the low-pressure operation limit. However, with regard to safety concerns and the early stage of development for NMP-001, the propellant injection time had to be restricted to 3.2–3.5 s. While this duration is sufficient for demonstrating burn times typical in RCS and DACS applications run in pulse operation mode, this does not adequately represent long-duration burns. Consequently, the test data had to be thoroughly analyzed to identify the onset of phenomena that could cause a shutdown during longer burn times than those tested. Each test was initially assigned a stability score of three points to evaluate both short- and long-duration combustion stability. An overview of the scoring system and rating criteria is presented in Table 6. Tests in which the monopropellant operation (t_3 to t_4) is shorter than 2 s are considered non-stable, which results in a subtraction of two points from the overall score. In cases where the monopropellant operation time is longer than 2 s, other stability criteria are applied.

The first rating criterion is based on the heating rate (HR) of the combustion chamber walls. Because a heatsink chamber was used, the wall heating rate should always be positive during a test. Therefore, a positive heating rate can serve as an indicator of long-duration burn combustion stability. Suppose the chamber wall is observed to be cooling down instead of heating up. In that case, it suggests that the combustion will likely be extinguished at some point in the future, even if this occurs after the regular experimental combustion time. Only sensors located in the lateral half of the combustion chamber (sensors 6 to 11) are considered for this metric in order to minimize the influence of the ignition procedure on this rating. A rapid heat transfer from the front half of the chamber to the lateral half is not expected to be prevalent because of the low heat conductivity of the stainless steel used as the combustor construction material. As shown in Fig. 6, the sensors located in the first half of the combustor register a "bump" during the ignition phase (at 1500–2200 ms), followed by a temperature drop during the monopropellant combustion phase, which could be caused by a propellant film cooling the chamber wall. In the lateral half of the combustor, which is significantly less affected by the ignitor and the injected propellant, the heating rate only changes slightly after the ignition sequence is over.

The heating rate is calculated within the w_1 window using Eq. (6). If the calculated heating is negative, the score is reduced by two points.

$$HR = \frac{\overline{T}_{6-11}(w_{1,\text{end}}; w_{1,\text{end}} - 100\,\text{ms}) - \overline{T}_{6-11}(w_{1,\text{start}}; w_{1,\text{start}} + 100\,\text{ms})}{w_{1,\text{end}} - w_{1,\text{start}}} \tag{6}$$

HR : Heating rate, [K/ms]
$\overline{T}_{6-11}$: Mean of sensor 6-11 readings inside a given interval, [K]
$w_{1,\text{start}}$: Starting value of window w_1, [ms]
$w_{1,\text{end}}$: Last value of window w_1, [ms]

The calculated heating rate is not expected to be affected by the measurement uncertainties arising from the ±2.5 K deviation caused by the used sensors because the underlying measurements are averaged over six sensor locations and throughout 100 ms. Additionally, it seems unlikely that all sensors deviate from measuring + 2.5 K to −2.5 K within the duration of w_1.

The third criterion used involves analyzing oscillations that occur during combustion. According to [55], rocket combustion is considered stable if the oscillations do not exceed ±5% of the average combustion chamber pressure at static operation. This paper calls this phenomenon "Oscillation Intensity" (OI). To evaluate this metric, the upper and lower envelopes of the pressure signal within the window w_1 are calculated (typically w_1 is set between 3000 to 4000 ms, as shown in Fig. 5). At least four points are used for each envelope. These points may not always be located at the beginning or end of the signal; therefore, the envelopes are extended along the first and last y-coordinates of the points. Even though the entire window w_1 is used for OI calculation, only the last part, i.e., the one corresponding with window w_2 (3750 to 4000 ms in this case), is used for evaluation. This approach allows the capture of changing dynamics or instabilities that may arise toward the end of the experiment. In the test shown in Fig. 7, the oscillation intensity was evaluated to be 5.67%. We consider tests with an OI higher than 5% stable for short-duration firings. However, long-duration combustion stability is questionable and must be evaluated in more extended test runs in further tests. Therefore, the stability score in high-OI tests is decreased by one point.

The oscillation intensity value is calculated using Eq. (7):

$$OI = \frac{max\{|\text{env}_{hi,t} - \overline{P}_{w1}|; |\text{env}_{low,t} - \overline{P}_{w1}|\}}{\overline{P}_{w1}}, \qquad \forall t \in w_1 \tag{7}$$

OI : Oscillation intensity, [%]
$\text{env}_{hi,t}$: Upper envelope value at t, [bar]
$\text{env}_{low,t}$: Lower envelope value at t, [bar]
$\overline{P}_{w1}$: Mean chamber pressure inside w_1, [bar]

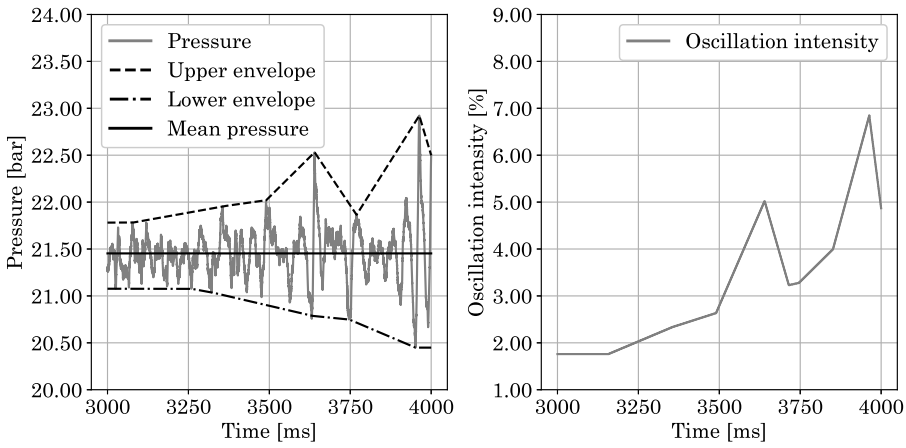

Fig. 7. Combustion oscillation intensity calculation.

Another criterion is used to account for longer-term tendencies in the combustion chamber pressure. Analogously to the oscillation intensity criterion, a rating deprecation by one occurs if the mean pressure drops more than 5% inside the w_1 window. The formula for calculating the pressure rate (PR) is similar to the one used for the heating rate and is given by Eq. (8):

$$PR = \frac{\overline{P}(w_{1,\text{end}}; w_{1,\text{end}} - 50\,\text{ms}) - \overline{P}(w_{1,\text{start}}; w_{1,\text{start}} + 50\,\text{ms})}{\overline{P}_{w1}} \tag{8}$$

PR : Pressure rate, [%]
$\overline{P}$: Mean chamber pressure inside a given interval, [bar]
$w_{1,\text{start}}$: Starting value of window w_1, [ms]
$w_{1,\text{end}}$: Last value of window w_1, [ms]

OI and PR are not affected by measurement uncertainties that stem from the combustion pressure sensor because both quantities are relative and calculated from a single measuring channel. As with the thermocouples, it is unlikely that the sensor offset would change from +0.5 bar to −0.5 bar within the w_1 window.

In order to evaluate the combustion efficiency, the measured characteristic velocity C^* (Eq. (9)) was compared to the theoretical value C^*_{CEA} calculated with the Gordon-McBride algorithm [39]. The comparison produces the efficiency value (10):

$$C^* = \frac{\overline{P}_{w2}}{\dot{m}_{w2}} \pi \frac{d_t^2}{4} \tag{9}$$

$$\eta_{C^*} = \frac{C^*}{C^*_{CEA}} \tag{10}$$

C^* : Characteristic velocity, [m/s]
$\overline{P}_{w2}$: Mean chamber pressure inside w_2, [MPa]
$\dot{m}_{w2}$: Mean propellant mass flow inside w_2, [kg/s]
d_t : Nozzle throat diameter, [mm]
η_{C^*} : Combustion efficiency, [%]
C^*_{CEA} : Calculated theoretical characteristic velocity, [m/s]

It is important to note that the C^* and η_{C^*} values are affected by uncertainties that stem from measurement inaccuracies. These were accounted for by considering error propagation as described by Diek [64]. For both C^* and η_{C^*}, the divergence was in the order of up to ±4.5%.

3. Results and discussion

3.1. Low-pressure combustion limit

The last stable load points of configuration C1 demonstrated stable chamber operation at a pressure of 15.0 to 15.6 bar. This test was carried out with the NMP-001 tank pressurized to 20 bar (see Fig. 8). Notably, this pressure is nearly half of what was reported by Kindsvater et al. for other nitromethane-based propellant formulations [47]. In the three following tests, tank pressure was set to 18 bar. However, only non-stable combustion could be achieved. These results determine the low-pressure operation limit to 15.1 bar, i.e., the average chamber pressure achieved during the last three functioning tests.

The last functioning load point (70 bar tank pressure) with test configuration C2 only yielded two data points. In both cases, stable combustion was achieved at 29.0 and 27.6 bar. The low-pressure combustion limit for this test configuration was thus determined to be 28.3 bar, the average pressure achieved at this load point. Tests at a tank pressure of 60 bar did not yield stable combustion. However, the flameout did not happen immediately after the igniter was switched off in two of the three "no-go"-tests. These tests only achieved 1.3 and 0.85 s stable monopropellant operation at 26.1 and 22.6 bar, respectively. Such combustion behavior hints at a gradual stable/non-stable regime change between the load points with 70 and 60 bar tank pressure, potentially proving the identified low-pressure combustion limit quite robust. Nevertheless, further tests with a tank pressure between 60 and 70 bar are desirable to cement the findings further.

In test configuration C3 at 27 bar tank pressure, stable operation at an average pressure of 16.5 bar could be achieved in four cases. However, two of these tests had an oscillation intensity of 5.6 and 5.9%, which questions the long-duration burn stability for these tests and hints that the low-pressure combustion limit is near. Nevertheless, it was decided to set the low-pressure combustion at this load point. Even though stable combustion was reached in one of the four experiments at 25 bar tank pressure, this load point was considered non-stable because stable combustion could not be repeated despite trying thrice.

Fig. 9 illustrates the influence of L^* on the low-pressure combustion limit. The low-pressure combustion limit depends on the characteristic chamber length and, consequently, the propellant residence time. This effect is attributed to the pressure-dependent nature of nitromethane's combustion mechanism (see [35–37]). If the combustion pressure is high, the decomposition and combustion reactions have enough time to complete and generate the heat required to support a self-sustaining combustion in a shorter chamber. If the pressure is low, more time is required for the chemical reactions to complete, and thus, a larger combustion chamber that provides for a longer residence time is required. However, Fig. 9 shows a potential saturation effect: extending the characteristic length beyond 7.2 to 7.5 m does not significantly affect the low-pressure operation limit. This L^* range could be interpreted as a preliminary design value for NMP-001 thrusters for spacecraft and satellites.

Another factor that could potentially affect the low-pressure combustion limit is the Sauter-Mean-Diameter of the droplets produced by

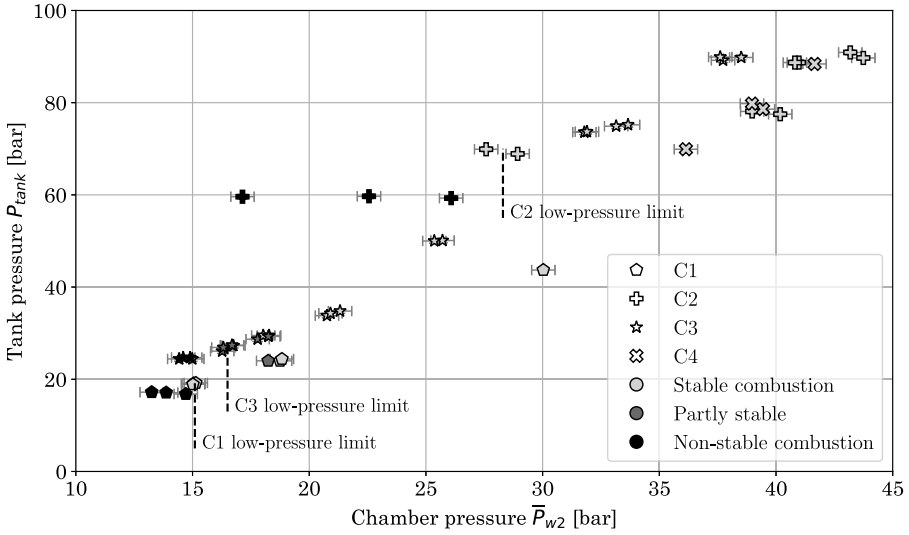

Fig. 8. Overview of the load points used in the test campaign.

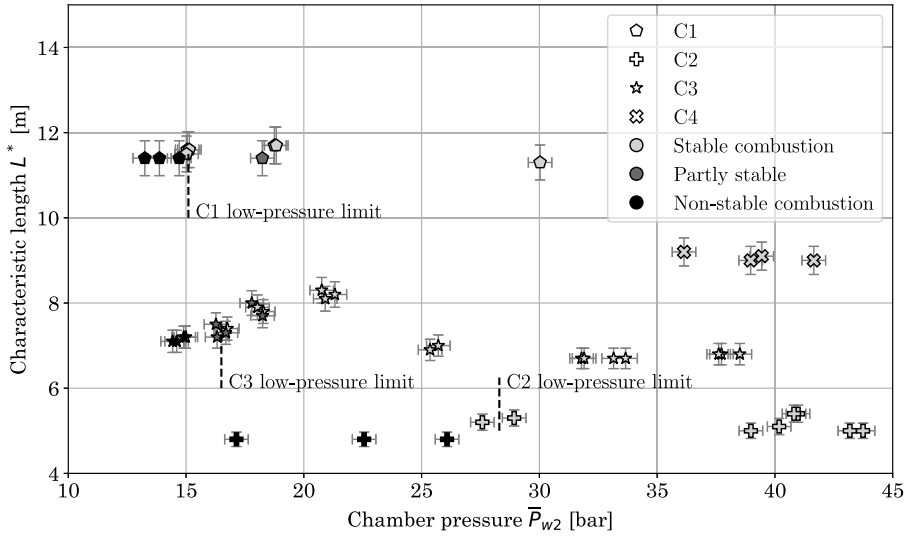

Fig. 9. Influence of the characteristic length on the low-pressure combustion limits.

the injector. The SMD was estimated from regressions of data points produced by laser interferometry measurements in cold-flow spray experiments conducted with water (see Fig. 4 and Section 2.3). Fig. 10 presents its effect on combustion stability and the low-pressure operation limit with NMP-001. Note that no error bars are present for SMD. This is because the SMD presented here is a rough estimation based on measurements carried out with a different (although similar) fluid than NMP-001 and not inside an enclosed, hot, and pressurized environment. With this caveat discussed, the SMD could still be a helpful variable for understanding the combustion behavior of NMP-001. At the low-pressure operation limit in the C1 test series, the highest SMD caused by the lowest injector pressure drop is prevalent. Because of this, it is impossible to tell if the flameouts are caused by the low combustion pressure, which is a crucial factor in nitromethane decomposition and combustion, or by a lack of proper propellant atomization. In the other two cases where a low-pressure combustion limit was identified, combustion pressure played the governing role, and the effect of the SMD was secondary.

The energy applied during the ignition procedure may be another source governing the combustion limit. Because of the different load points and test configurations used in this campaign, the ignition procedure had to be varied. Tuning the ignition sequence involved changing the boost oxygen feed pressure, the metering orifice, and varying the valve closure time (t_3) between 1800 and 2500 ms. Adjusting the injection point t_1 between 850 to 1700 ms was also necessary. These manipulations were required to provide for a guaranteed ignition in every load point characterized in this campaign. An additional factor that required changes to the ignition sequence was rooted in minor changes to the propellant, oxygen, and hydrogen lines caused by breaks between the test series.

Ultimately, the wall temperature rise between t_0 and t_3 (i.e., during the operation of the ignitor pilot chamber and the boost oxygen stage) represents the effect of the ignition sequence in the combustion process. Fig. 11 plots this temperature against the average chamber pressure in window w_2. The temperature is averaged over the last six sensors along the chamber axis for each data point to minimize effects due to possible propellant film formation and pilot-chamber-induced hot spots on the chamber wall in the front part of the chamber. No clear correlation between the temperature rise and low-pressure operation limit could be identified from the data presented in Fig. 11. In fact, in both the low-pressure combustion limit "no go" load point in C1 and the stable load point preceding it, only a ΔT of around 60–70 K was produced during the ignition process in the lateral half of the chamber. This value is one

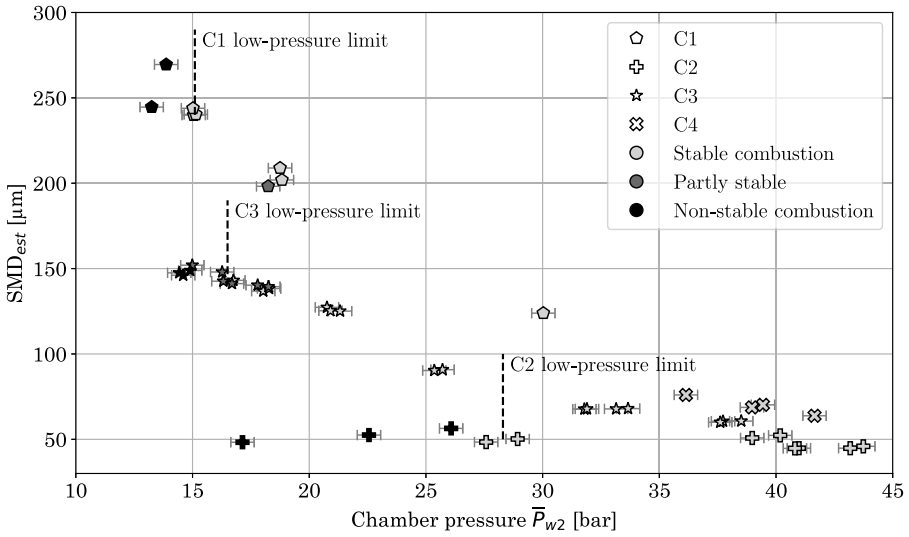

Fig. 10. Influence of the estimated Sauter-Mean-Diameter on the combustion stability.

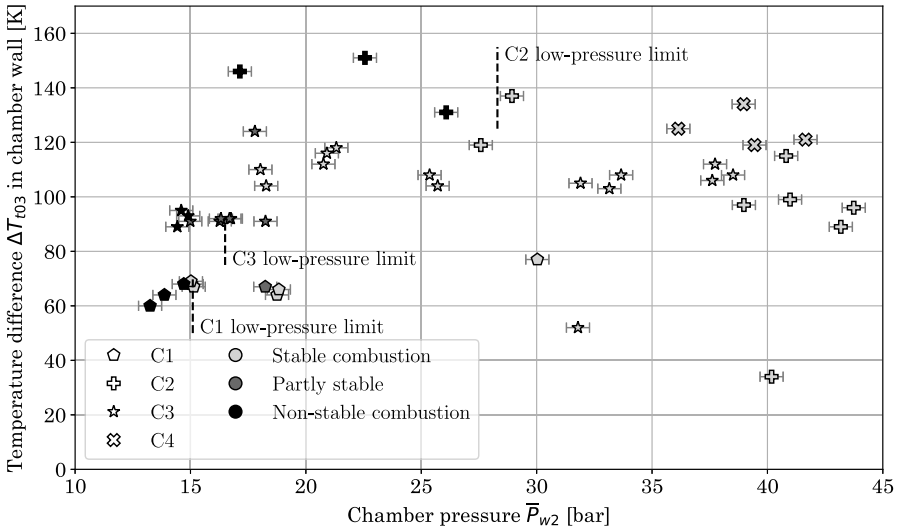

Fig. 11. Influence of chamber wall temperature (last six sensors along the chamber axis) after the ignition on low-pressure combustion limit.

of the lowest encountered in the test campaign — yet stable combustion was possible.

3.2. Combustion efficiency

Table 7 presents and quantifies the influence of the combustion pressure $\overline{P}w_2$ and the estimated droplet diameter SMD$_{est}$ on combustion efficiency η_{C^*}. To compare these effects on an "apples-to-apples" basis, each quantity Q is normalized using Eq. (11). For example, in the case of the combustion chamber pressure $\overline{P}_{w_2}$ in the C1 tests, this would mean assigning 0% to 15.0 bar and 100% to 30.0 bar.

$$Q_{norm} = \frac{Q - Q_{min}}{Q_{max} - Q_{min}} \times 100\% \tag{11}$$

Q : Data array
Q_{norm} : Normalized data array
Q_{max} : Maximal value in data array
Q_{min} : Minimal value in data array

For this investigation, only stable tests from each test series were used. Note that direct quantitative comparability of the influence factors is only ensured within a test series. Additionally, only if a quantity is changed by at least 50%[4] inside a data series is the data considered sufficiently spread out to allow for useful analysis. Therefore, in test series C2, only the influence of the combustion pressure is quantified, and the test series with configuration C4 is excluded from this analysis.

After normalizing, the data array is combined with the corresponding values for the combustion efficiency η_{C^*}, and eventually, a linear fit is made. The gradient in the fit can be interpreted as the effect of the quantity on the combustion efficiency.

Boyer et al. and Kelzenberg et al. [35,36] showed that the combustion pressure strongly influences the combustion rate of nitromethane in laboratory strand burners. Yetter et al. [37] attribute this to the pressure-dependent decomposition mechanism of nitromethane. Therefore, a higher combustion chamber pressure is expected to influence the reaction rate positively. As seen in Table 7 within test series C1 and C3, this also is the case: 0.070 and 0.091% efficiency increase per increase of the pressure range by one percentage point, respectively. In test series C2, the efficiency slightly decreases with increasing pressure, which is unexpected. However, because of its low magnitude, this

[4] That is if it is halved or increased by one and a half times.

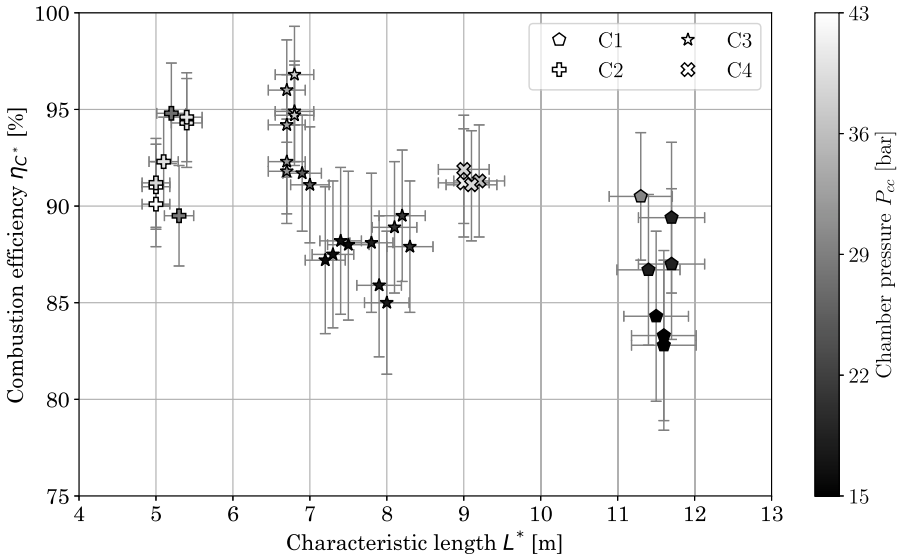

Fig. 12. Effect of the characteristic length L^* on the combustion efficiency.

Table 7
Influence of the combustion pressure $\overline{P}_{w2}$ and the estimated droplet diameter SMD_{est} on the combustion efficiency η_{C^*}.

	$\overline{P}_{w2}$ range [bar]	SMD_{est} range [μm]	η_{C^*} range [%]	Gradient of the $\overline{P}_{w2,norm}$-η_{C^*} fit $[\frac{\%\eta_{C^*}}{\%\overline{P}_{w2,norm}}]$	Gradient of the SMD_{est}-η_{C^*} fit $[\frac{\%\eta_{C^*}}{\%SMD_{est,norm}}]$
C1	15.0–30.0	123.6–243.6	82.8–90.5	0.070	−0.073
C2	27.6–43.7	44.7–52.3	89.5–94.8	−0.005	N/A
C3	16.3–38.5	60.0–148.0	85.0–96.8	0.091	−0.082
C4	36.1–41.7	63.8–76.0	91.1–91.9	N/A	N/A

decrease is considered to be rooted in random fluctuations of the test starting conditions, such as the ambient temperature, the chamber wall temperature, or variations in propellant compositions. Yet, more testing should be carried out to investigate further effects.

Another source of influence on combustion performance is considered to be the degree of propellant atomization, represented by SMD_{est}. In test series C1 and C3, the performance decreases by 0.073 and 0.082 percentage points for each one percentage point decrease in the SMD_{est} range. The quantitatively more substantial influence of SMD_{est} compared to the chamber pressure $\overline{P}w_2$ in test series C1 (0.073 vs. 0.070) supports the presumption that the non-stable combustion at propellant feed pressures of 18 bar, corresponding to chamber pressures below 15 bar, may have been caused by propellant accumulation due to insufficient atomization rather than a slow reaction rate at low chamber pressures. However, as the difference in influence SMD_{est} versus $\overline{P}_{w2}$ in C1 (and also in C3) is relatively small, a definitive prevalence of one phenomenon over the other cannot be conclusively determined. Therefore, further investigations are required where only one of the two possible influencing factors is varied.

The propellant residence time, represented by the characteristic length L^*, is also expected to influence combustion efficiency. Fig. 12 presents the combined effects of the characteristic length and the chamber pressure on combustion efficiency for all data points from the C1, C2, C3, and C4 test series. Overall, performance decreases with larger characteristic lengths L^*. This decrease is attributed to an increase in the thermal mass of the combustor. On the other hand, a larger characteristic length corresponds to an increased residence time, allowing the reaction to complete at lower pressures, albeit at the cost of decreasing efficiency.

According to Kelzenberg et al. [35], the burning rate of a nitromethane liquid column in a strand burner more than doubles from 20 to 40 bar pressure. In a strand burner, the combustion phenomenon is confined to only one dimension: the burning liquid surface. In a rocket motor, on the other hand, a propellant spray rapidly transformed into a vigorous turbulent gas-phase decomposition, and combustion can be regarded as a three-dimensional phenomenon. Therefore, it seems reasonable to assume that the reaction rate does not just double between low- and high-pressure tests described in this paper but possibly increases by an order of magnitude. This increase explains why values above 90% are only prevalent at pressures above 25 bar. The much more vigorous reaction compensates for the energy loss in the case of a characteristic length L^* of up to 9 m.

4. Conclusion

This paper investigates the combustion behavior of NMP-001. This monopropellant mainly consists of nitromethane and is enhanced with additives to enable low-pressure combustion and reduce sensitivity to mechanical stimuli. The conducted tests have unveiled a notable decrease in the low-pressure operational limit compared to reported values for pure nitromethane.

The presented test campaign employed four combustion chamber configurations, each with a different characteristic length. These configurations denoted as C1, C2, C3, and C4, utilized the same combustion chamber but had varying nozzle sizes. Because of erosion of the nozzle throat, the L^* values varied slightly, resulting in values of 11.3–11.7 m for C1, 4.7–5.4 m for C2, 6.7–8.3 m for C3, and 9.0–9.5 m for C4. The low-pressure combustion limit for the configurations C1, C2, and C4 was determined to be 15.1, 28.3, and 16.2 bar, respectively. Notably, especially in the case of the C1 and C3 test configurations, these values are significantly below the 30 bar limit reported for other nitromethane-based propellant formulations by Kindsvater et al. [47]. Despite using a heat-sink chamber combined with a simple 3D-triplet injector element and employing a non-optimized propellant formulation, a combustion efficiency ranging from 82.8% to 96.8% was achieved.

The characteristic chamber length was found to have the most significant effect on the low-pressure combustion limit (see Fig. 9). This effect is attributed to nitromethane's pressure-dependent reaction rate (see [35–37]): at high pressure, the rapid decomposition and combustion reactions only require a short residence time to complete, allowing for a small L^* value. At low pressures, however, the reactions require a longer time to complete, which leads to a high L^* requirement for stable low-pressure operation.

The effects of several factors that influence combustion efficiency were also investigated. At low pressures, the efficiency falls with increasing characteristic length because the capacitively cooled chamber walls absorb the energy. At pressures above 25 bar, the much higher reaction rate compensates and leads to a high combustion efficiency (up to 96.8%) even at L^*-values as high as 9 m, where the reaction rate compensates for the energy losses.

Fig. 9 shows a potential saturation effect, where stable low-pressure operation below 20 bar can be enabled at a characteristic length of 7.2 to 7.5 m. Extending this metric beyond this value does not significantly improve the low-pressure combustion limit. In conclusion, it can be inferred that this range represents a usable first working design value for NMP-001 thrusters intended for use in pressure-fed spacecraft and satellite propulsion systems.

In test configuration C1, the degree of atomization may also have played a role in determining both the low-pressure combustion limit and the combustion efficiency. At a chamber pressure of around 15 bar, i.e., at the last load point where stable combustion was achieved, the highest estimated Sauter-Mean-Diameter of the injector spray droplets encountered in this test campaign was prevalent. A too-coarsely atomized propellant spray may have led to the flameouts produced at the next lower-pressure operation point in tests with the C1 configuration. A low SMD_{est} might have contributed to a poor combustion efficiency of the last load point.

Even with NMP-001 being a prototype propellant, stable operation at pressures commonly used in satellite and spacecraft thrusters was demonstrated. Although the demonstrated C^*-performance of 1138 to 1330 m/s is not optimal, it is still comparable with the performance of LMP-103s (1372 m/s, see Fig. 1). Even though the H_2/O_2 torch ignitor proved reliable and did not influence the campaign results, from a system engineering perspective, relying on a bulky and cumbersome torch ignitor in satellite or spacecraft propulsion systems is undesirable. Therefore, there is a pressing need to develop alternative ignition methods better suited for this propellant's intended application.

CRediT authorship contribution statement

Maxim Kurilov: Writing – review & editing, Writing – original draft, Validation, Software, Project administration, Methodology, Investigation, Formal analysis, Data curation, Conceptualization. **Lukas Werling:** Writing – review & editing, Supervision. **Christoph Kirchberger:** Writing – review & editing, Supervision, Resources, Funding acquisition. **Helmut Ciezki:** Writing – review & editing, Writing – original draft. **Stefan Schlechtriem:** Supervision, Resources, Funding acquisition.

Declaration of competing interest

The authors declare that they have no known competing financial interests or personal relationships that could have appeared to influence the work reported in this paper.

Acknowledgments

The authors thank the DLR M11 technicians and engineers Nadine Stoll, Ingo Dörr, Hagen Friedrich, Jan Buddenberg, and Marius Wilhelm for providing excellent technical support for this test campaign. Prof. Dr. Simona Silvestri and Dr. Sebastian Klein also deserve our deepest gratitude for helping us find good answers to tough questions.

References

[1] European Chemicals Agency, Substance infocard - hydrazine, 2024, https://echa.europa.eu/de/substance-information/-/substanceinfo/100.005.560. (Accessed 1 May 2024).
[2] W.M. Marshall, M.C. Deans, Recommended figures of merit for green monopropellants, in: 49th AIAA/ASME/SAE/ASEE Joint PropulsionConference, 2013, p. 3722.
[3] V. Bombelli, D. Simon, J.-L. Moerel, T. Marée, Economic benefits of the use of non-toxic mono-propellants for spacecraft applications, in: 39th AIAA/ASME/SAE/ASEE Joint Propulsion Conference and Exhibit, 2003, p. 4783.
[4] M. Negri, M. Wilhelm, C. Hendrich, N. Wingborg, L. Gediminas, L. Adelöw, C. Maleix, P. Chabernaud, R. Brahmi, R. Beauchet, et al., New technologies for ammonium dinitramide based monopropellant thrusters–The project RHEFORM, Acta Astronaut. 143 (2018) 105–117.
[5] N. Wingborg, C. Eldsäter, H. Skifs, Formulation and characterization of ADN-based liquid monopropellants, in: A. Wilson (Ed.), Proceedings of the 2nd International Conference on Green Propellants for Space Propulsion (ESA SP-557). 7-8 June 2004, Chia Laguna (Cagliari), Sardinia, Italy, Vol. 557, CDROM, 2004, p. 16.1.
[6] M. Persson, K. Anflo, P. Friedhoff, Flight heritage of ammonium dinitramide (ADN) based high performance green propulsion (HPGP) systems, Propellants Explos. Pyrotech. 44 (9) (2019) 1073–1079.
[7] A. Dinardj, K. Anflo, P. Friedhoff, On-orbit commissioning of high performance green propulsion (HPGP) in the SkySat constellation, in: 31st AIAA, USU Conf. on Small Satellites, Utah, 2017, pp. SSC17–X–04.
[8] T. Katsumi, K. Hori, Successful development of HAN based green propellant, Energ. Mater. Front. 2 (3) (2021) 228–237.
[9] K. Hori, T. Katsumi, S. Sawai, N. Azuma, K. Hatai, J. Nakatsuka, HAN-based green propellant, SHP163–Its R&D and test in space, Propellants Explos. Pyrotech. 44 (9) (2019) 1080–1083.
[10] R.A. Spores, GPIM AF-M315E propulsion system, in: 51st AIAA/SAE/ASEE Joint Propulsion Conference, 2015, p. 3753.
[11] E. Wucherer, S. Christofferson, B. Reed, Assessment of high performance HAN-monopropellants, in: 36th AIAA/ASME/SAE/ASEE Joint Propulsion Conference and Exhibit, 2000, p. 3872.
[12] R.K. Masse, R. Spores, M. Allen, AF-M315E advanced green propulsion–GPIM and beyond, in: AIAA Propulsion and Energy 2020 Forum, 2020, p. 3517.
[13] C. Maleix, P. Chabernaud, R. Brahmi, R. Beauchet, Y. Batonneau, C. Kappenstein, M. Schwentenwein, R.-J. Koopmans, S. Schuh, C. Scharlemann, Development of catalytic materials for decomposition of ADN-based monopropellants, Acta Astronaut. 158 (2019) 407–415.
[14] P. Gonzalez Rueda Flores, R.A. Cuevas, A. Rahman, R.A. Zubia, E.A. Tobias, S.C. Adams, N. Ontiveros, J. Quintana, A.D. Greig, A.R. Choudhuri, Implementing test methodology improvements for testing and validation of a 1N AF-M315E thruster, in: AIAA Propulsion and Energy 2021 Forum, 2021, p. 3590.
[15] M. Kilcoin, D. Cavender, T. Hasanof, M. Zaluki, T. McKechnie, C. Sedano, H. Williams, Development of ASCENT propellant thrusters and propulsion systems, 2022.
[16] R.K. Masse, B.A. Glassy, R.A. Spores, A.T. Vuong, Z. Zhu, T.L. Pourpoint, Hydrazine-based green monopropellant blends, in: AIAA SCITECH 2024 Forum, 2024, p. 1619.
[17] U. Gotzig, Challenges and economic benefits of green propellants for satellite propulsion, in: 7th European Conference for Aeronautics and Space Sciences, EUCASS, 2017.
[18] Digital Solid State Propulsion Inc., Chemicals and propellants - AF-M315E pricing, 2024, https://dsspttech.com/propellant-products. (Accessed 4 January 2024).
[19] A. Sarritzu, L. Felix, W. Lukas, A. Pasini, Assessment of propulsion system architectures for green propellants-based orbital stages, in: International Astronautical Congress: IAC Proceedings, IAF (International Astronautical Federation), 2022.
[20] M. Ventura, E. Wernimont, S. Heister, S. Yuan, Rocket grade hydrogen peroxide (RGHP) for use in propulsion and power devices-historical discussion of hazards, in: 43rd AIAA/ASME/SAE/ASEE Joint Propulsion Conference & Exhibit, 2007, p. 5468.
[21] F. Massimo, Safety evaluation and experience of hydrogen peroxide in launchers domain at Guiana Space Centre, in: Space Safety is No Accident: The 7th IAASS Conference, Springer, 2015, pp. 169–178.
[22] V. Syromiantikov, C.J. Faranetta, The Soyuz spacecraft today and tomorrow, in: Proceedings of the Elventh SSI/Princeton Conference on Space Manufacturing, Springer, 1997, pp. 144–147.
[23] M. Wade, Soyuz, 2019, (Accessed 18 January 2024). URL http://www.astronautix.com/s/soyuz.html.
[24] A. Pasini, L. Sales, E. Puccinelli, L. Lin, A. Apollonio, R. Simi, G. Brotini, L. d'Agostino, Design of an affordable hydrogen peroxide propulsion system for CubeSats, in: AIAA Propulsion and Energy 2021 Forum, 2021, p. 3690.
[25] P. Surmacz, M. Kostecki, Z. Gut, A. Olszyna, Aluminum oxide–supported manganese oxide catalyst for a 98% hydrogen peroxide thruster, J. Propuls. Power 35 (3) (2019) 614–623.

[26] B.J. German, E.C. Branscome, A.P. Frits, N.C. Yiakas, D.N. Mavris, An evaluation of green propellants for an ICBM post-boost propulsion system, in: Missile Sciences Conference, 2000.
[27] M. Ventura, Long term storability of hydrogen peroxide, in: 41st AIAA/ASME/SAE/ASEE Joint Propulsion Conference & Exhibit, 2005, p. 4551.
[28] E. Boyer, K. Kuo, Characteristics of nitromethane for propulsion applications, in: 44th AIAA Aerospace Sciences Meeting and Exhibit, 2006, p. 361.
[29] J.D. Clark, Ignition!: An Informal History of Liquid Rocket Propellants, Rutgers University Press, 1972.
[30] W.C. House, Project SQUID. Filed survey report, Liq. Propellant Rockets 2 (2) (1947).
[31] A. Hermoni, Role of rate of decomposition of nitric oxide in the use of nitromethane as a monopropellant, J. Appl. Chem. 9 (8) (1959) 420–422.
[32] A. Makovky, L. Lenji, Nitromethane-physical properties, thermodynamics, kinetics of decomposition, and utilization as fuel, Chem. Rev. 58 (4) (1958) 627–644.
[33] J.B. Benziger, Decomposition of nitromethane over NiO and Cr2O3 catalysts, Combust. Sci. Technol. 29 (3–6) (1982) 191–205, http://dx.doi.org/10.1080/00102208208923597, arXiv:https://doi.org/10.1080/00102208208923597.
[34] J.B. Benziger, A mechanistic study of nitromethane decomposition on nickel, Appl. Surf. Sci. 17 (3) (1984) 309–323.
[35] S. Kelzenberg, N. Eisenreich, W. Eckl, V. Weiser, Modelling nitromethane combustion, Propellants Explos. Pyrotech. 24 (3) (1999) 189–194.
[36] E. Boyer, K.K. Kuo, Modeling of nitromethane flame structure and burning behavior, Proc. Combust. Inst. 31 (2) (2007) 2045–2053.
[37] R.A. Yetter, V. Yang, M.H. Wu, Y. Wang, D. Milius, I.A. Aksay, F.L. Dryer, Combustion issues and approaches for chemical microthrusters, Int. J. Energ. Mater. Chem. Propuls. 6 (4) (2007).
[38] C.D. Brown, Spacecraft Propulsion, Aiaa, 1996.
[39] S. Gordon, B.J. McBride, Computer Program for Calculation of Complex Chemical Equilibrium Compositions and Applications. Part 1: Analysis, Tech. rep., NASA Lewis Research Cente, 1994.
[40] I. Digital Solid State Propulsion, AF-M315E safety data sheet, 2024, https://dssptech.com/propellant-products.
[41] K. Anflo, R. Möllerberg, Flight demonstration of new thruster and green propellant technology on the PRISMA satellite, Acta Astronaut. 65 (9–10) (2009) 1238–1249.
[42] D. Freudenmann, H.K. Ciezki, ADN and HAN-based monopropellants–a minireview on compatibility and chemical stability in aqueous media, Propellants Explos. Pyrotech. 44 (9) (2019) 1084–1089.
[43] M. Kurilov, L. Werling, M. Negri, C. Kirchberger, S. Schlechtriem, Impact sensitivity of nitromethane-based green-propellant precursor mixtures, Int. J. Energ. Mater. Chem. Propuls. 22 (2) (2023).
[44] B. Elvers, et al., Ullmann's Encyclopedia of Industrial Chemistry, vol. 17, Verlag Chemie, Hoboken, NJ, 1991.
[45] D.R. Lide, CRC Handbook of Chemistry and Physics, vol. 85, CRC Press, 2004.
[46] F. Bellinger, H. Friedman, W. Bauer, J. Eastes, J. Gross, Chemical propellants. mononitromethane, Ind. Eng. Chem. 40 (7) (1948) 1324–1331.
[47] H. Kindsvater, K. Kendall, K. Mueller, P. Datner, Research on Nitromethane, Report (493), Aeroject Engineering Cooperation, 1951.
[48] K.P. Shrestha, N. Vin, O. Herbinet, L. Seidel, F. Battin-Leclerc, T. Zeuch, F. Mauss, Insights into nitromethane combustion from detailed kinetic modeling–Pyrolysis experiments in jet-stirred and flow reactors, Fuel 261 (2020) 116349.
[49] M. Kurilov, L. Ziemer, V. Weiser, S. Ricker, C. Kirchberger, S. Schlechtriem, Ignition of nitromethane-based propellant mixtures, Int. J. Energ. Mater. Chem. Propuls. 23 (1) (2024).
[50] A. Campbell, M. Malin, T. Holland, Temperature effects in the liquid explosive, nitromethane, J. Appl. Phys. 27 (8) (1956) 963.
[51] M. Kurilov, C. Kirchberger, D. Freudenmann, A.D. Stiefel, H. Ciezki, A method for screening and identification of green hypergolic bipropellants, Int. J. Energ. Mater. Chem. Propuls. 17 (3) (2018).
[52] D. Suslov, A. Woschnak, J. Sender, M. Oschwald, O. Haidn, Test specimen design and measurement technique for investigation of heat transfer processes in cooling channels of rocket engines under real thermal conditions, in: 39th AIAA/ASME/SAE/ASEE Joint Propulsion Conference and Exhibit, 2003, p. 4613.
[53] L. Werling, T. Hörger, Experimental analysis of the heat fluxes during combustion of a N_2O/C_2H_4 premixed green propellant in a research rocket combustor, Acta Astronaut. 189 (2021) 437–451.
[54] T.W. Khan, I. Qamar, Optimum characteristic length of gas generator for liquid propellant rocket engine, Acta Astronaut. 176 (2020) 1–12.
[55] G.P. Sutton, O. Biblarz, Rocket Propulsion Elements, eighth ed., John Wiley & Sons, 2010.
[56] S. Gordon, B.J. McBride, Finite Area Combustor Theoretical Rocket Performance, Tech. rep., NASA Lewis Research Center, 1988.
[57] C. Inoue, T. Watanabe, T. Himeno, Atomization and flow characteristics of liquid sheet produced by jet impingement, J. Propuls. Power 28 (5) (2012) 1060–1070.
[58] H. Hiroyasu, M. Arai, Structures of fuel sprays in diesel engines, SAE Trans. (1990) 1050–1061.
[59] H. Ryan, W. Anderson, S. Pal, R. Santoro, Atomization characteristics of impinging liquid jets, J. Propuls. Power 11 (1) (1995) 135–145.
[60] E. Ibrahim, A. Przekwas, Impinging jets atomization, Phys. Fluids A 3 (12) (1991) 2981–2987.
[61] H. Ciezki, T. Tiedt, J. Von Kampen, N. Bartels, Atomization behavior of Newtonian fluids with an impinging jet injector in dependence upon Reynolds and weber numbers, in: 41st AIAA/ASME/SAE/ASEE Joint Propulsion Conference & Exhibit, 2005, p. 4477.
[62] G. Bailardi, M. Negri, H. Ciezki, Several aspects of the atomization behavior of various newtonian fluids with a like-on-like impinging jet injector, in: Proc. 23rd European Conf. on Liquid Atomization and Spray Systems, Brno, Czech Republics, 2010.
[63] W.-H. Lai, T.-H. Huang, T.-L. Jiang, W. Huang, Effects of fluid properties on the characteristics of impinging-jet sprays, At. Sprays 15 (4) (2005).
[64] R.H. Dieck, Measurement Uncertainty: Methods and Applications, ISA, 2007.